Anisotropy of stress correlation in two-dimensional liquids and a pseudospin model

Bin Wu, Takuya Iwashita, and Takeshi Egami

Phys. Rev. E **92**, 052303 — Published 4 November 2015

DOI: 10.1103/PhysRevE.92.052303

ANISOTROPY OF STRESS CORRELATION IN TWO-DIMENSIONAL LIQUIDS AND A PSEUDOSPIN MODEL

Bin Wu[1], Takuya Iwashita[2], Takeshi Egami[1,2,3,*]

1, Department of Physics and Astronomy, Joint Institute of Neutron Science, University of Tennessee, Knoxville, Tennessee 37996, USA

2, Department of Materials Science and Engineering, University of Tennessee, Knoxville, Tennessee 37996, USA

3, Oak Ridge National Laboratory, Oak Ridge, Tennessee 37831, USA

* To whom correspondence should be addressed: egami@utk.edu

Abstract

Liquids are condensed-matter in which atoms are strongly correlated in position and momentum. The atomic pair density function (PDF) is used often in describing such correlation. However, elucidation of many properties requires higher degrees of correlation than the pair correlation. For instance viscosity depends upon the stress correlations in space and time. In this paper, we examine the cross-correlation between the stress correlation at the atomic level and the PDF for two-dimensional liquids. We introduce the concept of the stress-resolved pair distribution function (SRPDF) that uses the sign of atomic level stress as a selection rule to include particles from density correlations. The connection between SRPDFs and stress correlation function is explained through an approximation in which the shear stress is replaced by a pseudospin. We further assess the possibility of interpreting the long-range stress correlation as a consequence of short-range Ising-like pseudospin interactions.

I. Introduction

In liquid atoms are strongly correlated in position and momentum, although its structure and dynamics appear to be random and chaotic. Therefore hidden physics is often unveiled through spatiotemporal correlation analysis of thermally activated fluctuations. The pair distribution function (PDF), $g(\vec{r})$, is a typical example of describing density correlation. Statistically $g(\vec{r})$ quantifies the probability of finding other particles at position $\vec{r}$ with respect to a central reference particle [1, 2]. Because the liquid is isotropic without external shear, the PDF is often denoted as $g(r)$ where $r = |\vec{r}|$. The PDF of liquids has been extensively investigated using scattering experiments [3, 4], computer simulations [5], and theories [6], for instance through the Ornstein-Zernike relation [1, 2], and serves as one of the key parameters to characterize atomic correlation [1, 2].

In contrast to the well-studied PDF less progress has been made in understanding the physics underlying correlation in shear stress fluctuations, even though the temporal correlation of macroscopic shear stress fluctuation is directly connected to shear viscosity through the Green-Kubo formula, and a number of works are published regarding shear viscosity calculations based on this formula [7-12]. By decomposing the macroscopic shear stress into the contributions from each atom [13], it can be found that the shear viscosity is given by the integration of spatiotemporal correlation of atomic level shear stresses [14]. Because the atomic-level stress depends on the relative positions of an atom at the center and the interacting neighbors, the atomic-level stress correlation represents a four particle density correlation.

Based on the decomposition of the macroscopic stress correlation into atomic-level stress correlations, Levashov *et al.* [14, 15] investigated the relationship between shear stress correlations and viscosity in *r*-space, while Furukawa and Tanaka [16, 17] approached this

problem in reciprocal space. Both studies concluded that viscosity has a non-local nature suggesting that the correlations among atomic level shear stresses are long-ranged. However the microscopic origin of stress correlation in liquids and its underlying physics remains unclear. For example, the stress correlation function shows prominent oscillations as a function of r, reflecting the atomic structure [14, 15]. For this reason, in some studies of amorphous solids [18-21], they use coarse-grained stress in order to approach a continuum limit and enhance applicability of elasticity theory [22, 23]. In this study we focus on the relationship between these oscillations and the PDF.

Recently we demonstrated that in two-dimensional liquids the spatial correlations among atomic level stresses are extended and anisotropic [24]. In this article we further investigate the microscopic origin of the observed stress correlation from the perspective of cross-correlation between atomic level stress and density fluctuations. We introduce the concept of the stress-resolved pair distribution functions (SRPDFs) which employ the sign of a specific stress component as a selection rule on the particles and decomposes the isotropic PDF into the SRPDFs. Here we use x-y shear stress as the stress component as an example to demonstrate the concept.

This paper is organized as follows. In Sec. II, we describe our MD simulation setup and data analysis methods which are used in calculating the atomic level stress and the SRPDFs. In Sec. III, we present the results of the SRPDFs and analyze their anisotropy through spherical harmonics expansion. We connect the stress correlation function and SRPDFs through representing the atomic level stress as quantized pseudospins, and develop an Ising-like pseudospin model with anisotropic exchange interaction to understand stress correlation in Sec. IV. Finally we present conclusions in Sec. V.

II. Methods

We ran molecular dynamics simulations [25] in two dimensions using the LAMMPS code [26]. We simulated monoatomic particles interacting through the pair-wise Yukawa potential that can be expressed as $V(r) = U_0 \frac{\sigma}{r} \exp(-\lambda \frac{r-\sigma}{\sigma})$. We used the Lennard-Jones (LJ) units, where the potential parameters σ, U_0, and mass of a particle m define the units of length, energy, and mass. In all runs, U_0 = 1, σ = 1, λ = 8, and m = 1. We employed a rectangular simulation box with the aspect ratio of $2:\sqrt{3}$ and applied periodic boundary conditions in both directions. All simulation runs of 2500 particles were conducted under the NVT ensemble with the number density fixed at 1.15. Under these settings, the melting temperature is found to be around T^* = 0.9 and the system forms liquids at temperatures beyond 1. For further details concerning the MD simulation setup, we refer to Ref. [24].

We use the atomic level stress to assess the local stress state of each particle and further examine its fluctuations. Its calculation follows the equation below [13]:

$$\sigma_i^{\alpha\beta} = \frac{1}{A_i} \sum_j \frac{dV(r_{ij})}{dr_{ij}} \frac{r_{ij}^{\alpha} r_{ij}^{\beta}}{r_{ij}}, \tag{1}$$

where the subscript represents the identity of the particle and the superscript means the corresponding Cartesian components. For instance, r_{ij}^x denotes the distance between particles i and j along the x-axis direction, and A_i is the atomic area of particle i, which could be evaluated from Voronoi analysis. However, for the sake of convenience, we replaced it with the average

area $\frac{A}{N}$, where A is the total area of the simulation box and N is the total number of particles. The summation over j is limited to particles inside a circle centered at particle i with the radius being the cutoff distance for force evaluation. We note that the kinetic contributions to the stress tensors are ignored because they are negligibly small comparing to the virial terms in Eq. 1 under the conditions studied here.

We restate the definition of the spatial stress correlation function introduced in Ref. [24]. Again we employ the autocorrelation of x-y shear stresses, which is listed below:

$$C(\vec{r}) = \left\langle \frac{\sum_i \sum_{j}^{j \neq i} \sigma_i^{xy} \sigma_j^{xy} \delta(\vec{r} - \vec{r}_i + \vec{r}_j)}{\sqrt{\sum_i \left(\sigma_i^{xy}\right)^2} \sqrt{\sum_j \left(\sigma_j^{xy}\right)^2}} \right\rangle . \quad (2)$$

We introduce the stress resolved pair distribution function (SRPDF) that is based on the sign of the atomic level stress. Since the atomic level stress is a tensor quantity, various SRPDFs can be defined through different choices of stress tensor elements. In this study, we chose the x-y shear stress as the specific stress component and hence

$$g_{+,0}(\vec{r}) = \left\langle \frac{2A}{N^2} \sum_{i}^{i \in \sigma_i^{xy} > 0} \sum_{j}^{j \neq i} \delta(\vec{r} - \vec{r}_i + \vec{r}_j) \right\rangle . \quad (3)$$

The first argument in the subscript of $g_{+,0}(\vec{r})$ indicates that only the particles that have positive x-y shear stress, *i.e.* $\sigma_i^{xy} > 0$, are selected as the reference particles while the second argument 0 means no selection rules are applied to surrounding particles for correlation. Therefore $g_{+,0}(\vec{r})$

quantifies the packing pattern of particles around a central particle with positive *x*-*y* shear stress. In the similar manner, the definitions of other SRPDFs, such as $g_{-,+}(\vec{r})$, are also straightforward.

III. Results

In Fig. 1, we present $g_{+,0}(r,\theta)$, where $r=|\vec{r}|$ and θ is the polar angle, computed for the liquid phase at temperature of 1. In panel (a), the result is illustrated in the form of two-dimensional contour plot, where the color represents the intensity. It is first noticed that an ellipse at the center is stretched along the $x = y$ direction and contracted in the other diagonal direction. This ellipse suggests that the nearest neighbor cage around a particle with positive *x*-*y* shear stress is non-circular. This observation is consistent with the previous understanding that the atomic level stress originates from the mismatch between the sizes and shapes of a particle and its nearest neighbor cage [13, 27-31], and in the glassy state the stress state can be modeled by the continuum elasticity theory by Eshelby [32]. In this specific example, the nearest neighbor cage is distorted from a circle with elongation in the $x = y$ direction and shrinkage in the $x = -y$ direction, while the shape of the central particle is circular. As a result of this misfit between the central particle and the host cage the central particle experiences a shear stress. The sign of the shear stress is determined by the direction of distortion of the neighbor cage. For instance, if the neighbor cage distortion is in the opposite manner, 90^{o} away, the shear stress of the central particle should be negative.

In panel (b) of Fig. 1, we show the intensity along three representative directions. In this representation, the distortion of the nearest neighbor cage is reflected by the systematic shifts of respective first peaks. For example, the first peak of $g_{+,0}(\vec{r})$ along the polar angle $\theta = 45^{o}$

direction is pushed outwards and that along $\theta = 135^{o}$ direction is contracted inwards. It is interesting to note that the systematic shifts of peaks are not limited to the first peaks but extends to long range. We performed the spherical harmonics expansion on $g_{+,0}(\vec{r})$ following the standard approach listed below:

$$g_{+,0}(\vec{r}) = \sum_{l,m} g_{+,0}^{l,m}(r) Y^{l,m}(\frac{\vec{r}}{|\vec{r}|}), \tag{4}$$

where $Y^{l,m}$ is the spherical harmonic function of degree l and order of m. More details concerning the spherical harmonics expansion on the PDF are shown in Appendix A. It is found that the relevant modes are $g_{+,0}^{0}(r)$ (isotropic) and $g_{+,0}^{2,-2}(r)$ (sin(2θ) symmetry). We show that $g_{+,0}^{0}(r)$ is identical to $g(r)$ for all particles and $g_{+,0}^{2,-2}(r)$ is proportional to $\frac{dg(r)}{dr}$ after the second positive peak with some phase shift in panels (a) and (b) of Fig. 2 respectively. Based on these observations, we formulate

$$g_{+,0}(\vec{r}) \approx g(r) - a\frac{dg(r+b)}{dr}\sin(2\theta), \tag{5}$$

where a accounts for scaling between $g_{+,0}^{2,-2}(r)$ and $\frac{dg(r)}{dr}$ while b is for their phase shift. Both of these two parameters assume the dimension of length. At the temperature of 1, we found a = 0.032 and b = 0.060. Since $g(r) = \frac{1}{2}\left[g_{+,0}(\vec{r}) + g_{-,0}(\vec{r}) \right]$, one can expect that $g_{-,0}(\vec{r}) \approx g(r) + a\frac{dg(r+b)}{dr}\sin(2\theta)$. This relationship was indeed confirmed by our calculations.

We next further decompose $g_{+,0}(\vec{r})$ by imposing a second selection criterion on the surrounding particles based on the signs of their atomic level *x*-*y* shear stresses. Under this decomposition scheme, $g_{+,0}(\vec{r}) = \frac{1}{2}\left[g_{+,+}(\vec{r}) + g_{+,-}(\vec{r}) \right]$. We illustrate the contour plots of $g_{+,+}(\vec{r})$ and $g_{+,-}(\vec{r})$ in panels (a) and (b) of Fig. 3. We see that $g_{+,+}(\vec{r})$ exhibits qualitatively similar anisotropy as that of $g_{+,0}(\vec{r})$ while $g_{+,-}(\vec{r})$ is almost isotropic.

Spherical harmonics expansions on $g_{+,+}(\vec{r})$ indicate that there are three relevant modes, namely $g_{+,+}^{0}(r)$ (isotropic), $g_{+,+}^{2,-2}(r)$ (sin(2θ) symmetry), and $g_{+,+}^{4,4}(r)$ (cos(4θ) symmetry). On the other hand, the nontrivial modes of $g_{+,-}(\vec{r})$ are $g_{+,-}^{0}(r)$ and $g_{+,-}^{4,4}(r)$, because $g_{+,-}^{2,-2}(r) = 0$ by symmetry. The comparisons between various modes of $g_{+,+}(\vec{r})$ and $g_{+,-}(\vec{r})$ are demonstrated in Fig. 4. It is found that $g_{+,+}^{2,-2}(r) = 2g_{+,0}^{2,-2}(r)$ and $g_{+,+}^{4,4}(r) = -g_{+,-}^{4,4}(r)$. The first equality suggests that the twofold-symmetry component of $g_{+,0}(\vec{r})$ exclusively stems from $g_{+,+}(\vec{r})$ (panel (b) of Fig. 4), while the second equality is expected because no fourfold-symmetry component is found in the sum of $g_{+,+}(\vec{r})$ and $g_{+,-}(\vec{r})$ (panel (c) of Fig. 4). It should be noted that $g_{+,+}^{0}(r)$ is slightly different from $g_{+,-}^{0}(r)$ as shown in panel (a) of Fig. 4. One can see that peak-heights are different up to the second peak and the long-range peaks show minor misalignment, which is hardly discernible from the plot.

IV. Pseudospin Model

In this section, we first establish a connection between the stress correlation function $C(\vec{r})$ and SRPDFs by simplifying atomic level stresses as quantized pseudospins. Then we further develop a simple Ising-like pseudospin model which may help elucidate the microscopic origin of stress correlations.

As far as the anisotropy of stress correlation function is concerned, the sign of the atomic level stress is more important than its absolute magnitude. This hypothesis will find strong support from the results that are shown below. Furthermore Langer suggested the Ising model could describe the mesoscopic ordering in liquids [33]. Following this idea, we approximate atomic level *x*-*y* shear stress as quantized Ising pseudospins that only adopt one of two states, namely

$$s_i = \begin{cases} 1, & if \quad \sigma_i^{xy} > 0. \\ -1, & if \quad \sigma_i^{xy} < 0. \end{cases} \tag{6}$$

Consequently the stress correlation function $C(\vec{r})$ in Eq. 2 can be approximated as

$$C(\vec{r}) \approx \frac{1}{N}\left\langle \sum_i \sum_{j}^{j \neq i} s_i s_j \delta(\vec{r} - \vec{r}_i + \vec{r}_j) \right\rangle , \tag{7}$$

where we employed an equality that $\sum_i (s_i)^2 = N$. Because the product of s_i and s_j equals 1 when they bear the same signs and -1 otherwise, Eq. 7 can be further reorganized as

$$C(\vec{r}) \approx \frac{N}{A} \Gamma(\vec{r}), \tag{8}$$

where

$$\Gamma(\vec{r}) = \frac{1}{4}\left[g_{+,+}(\vec{r}) - g_{+,-}(\vec{r}) + g_{-,-}(\vec{r}) - g_{-,+}(\vec{r}) \right]. \quad (9)$$

It is important to note that the above derivation also relies on a fact that statistically there are equal numbers of particles with positive and negative *x*-*y* shear stresses. Therefore we see that the stress correlation function is a linear combination of SRPDFs under the pseudospin approximation. We further define the spherical harmonics expansion of $\Gamma(\vec{r})$, $\Gamma^{l,m}(r)$. We present the contour plots of $C(\vec{r})$ calculated via Eq. (2) and $\Gamma(\vec{r})$ in panels (a) and (b) of Fig. 5 respectively. Resemblance between the two plots is remarkable. The quantitative comparison is shown in Fig. 6. We compare the isotropic mode of $\Gamma(\vec{r})$ versus the counterpart of $C(\vec{r})$ in panel (a) and their cos(4θ) modes in panel (b). The quantitative agreements are superb in terms of the shapes, heights and positions of the peaks. Nonetheless we see subtle deviations which are apparently attributable to the pseudospin approximation. We emphasize that these deviations are small but physically important. For example, the spatial integration of $\Gamma^0(r)$ is zero because statistically there are equal numbers of particles that have positive and negative *x*-*y* shear stresses, while on the other hand the spatial integration of $C^0(r)$ is proportional to shear modulus. This implies that the shear modulus of a liquid is nonzero due to the deviation from pseudospin approximation. This point will be discussed elsewhere in future publications.

The results above prove that the pseudospin approximation is reasonable as far as the extent and anisotropy of stress correlation are concerned. This approximation then naturally presents a possibility to interpret the long-range stress correlation as the consequence of Ising-like short-range interaction among pseudospins. To explore this possibility, we develop the following Ising-like pseudospin model. We assume that the state of a pseudospin is driven by

inter-pseudospin interaction and thermal excitation. The nature of this interaction is pairwise and short-ranged. Under this assumption, one viable form of Hamiltonian is

$$H = -\sum_{i} \sum_{j}^{j \neq i, r_{ij} < r_c} J_2 \sin 2\theta_{ij} \left(s_i + s_j \right) s_i s_j \ , \tag{10}$$

where r_c is the interaction range of pseudospins while J_2 represents the anisotropic exchange energy.

Within this framework, we carried out Monte Carlo (MC) simulation to test the pseudospin spin model. We used MD simulation trajectory for the positions of pseudospins. We assumed J_2 = -2.5 in the LJ unit and r_c equals the position of the first peak of the isotropic PDF, namely r_c = 0.93 at T^* = 1. The initial states of pseudospins were assigned random and the acceptance of flipping a randomly chosen pseudospin was based on the Metropolis method [25]. Once the total energy reached a steady value, we computed the pseudospin-resolved PDF (PRPDF) in the same fashion of calculating SRPDFs. For example,

$$S_{+,+}(\vec{r}) = \frac{4A}{N^2} \left\langle \sum_{i}^{s_i>0} \sum_{j}^{j \neq i, s_j>0} \delta(\vec{r} - \vec{r}_i + \vec{r}_j) \right\rangle \ . \tag{11}$$

Their spherical harmonic expansions are also straightforward. We present various modes of $S_{+,+}(\vec{r})$ and $S_{+,-}(\vec{r})$ at T^* = 1 in Fig. 7 comparing with their counterparts of SRPDFs shown previously in Fig. 4. In the same manner of determining the screening length from stress correlation function introduced in Ref. [24], the magnitude of the 4-fold component of pseudospin correlation function normalized by isotropic PDF is fitted with the screened Eshelby function,

$$\frac{|S_4(r)|}{g(r)} \approx \frac{B}{r^2}\exp\left(-\frac{r}{\xi}\right). \tag{12}$$

where $S_4(r) = 2S^{4,4}_{+,+}(r)$, B and ξ are the fitting parameters. In Fig. 8 we show the temperature dependence of the screening length, ξ. Again ξ follows a power law behavior of $\xi(T^*) = \xi_0(T^* - T_0)^{-\alpha}$ with T_0 = 0.74 and α = 0.82, which are fairly close to their counterparts from the stress correlation function, namely T_0 = 0.48 and α = 0.72. Even though we chose the simplest model with no account of other modes, *i.e.* the isotropic exchange, $\sum_{i,j} J_0 s_i s_j$, and the l = 4 interaction, $\sum_{i,j} J_4 \cos 4\theta_{ij} s_i s_j$, agreement is already reasonable. Inclusion of J_4 is likely to improve agreement. Nonetheless, the important outcome is that the simple short-range anisotropic Ising-like pseudospin interaction indeed can yield long-range correlation with the correct anisotropy. Therefore this Ising-like pseudospin model could be a viable option to model the microscopic stress correlation.

V. Conclusion

In this paper, we examined the cross-correlation between density and stress fluctuations through stress-resolved pair distribution functions, which employ the sign of the *x*-*y* shear stress as the selection criteria for choosing particles before the density correlation analysis. It is found that these SRPDFs have sin(2θ) or (and) cos(4θ) symmetry (symmetries). Through spherical harmonics expansion, we found that the twofold-symmetry component exhibits close connection with the derivative of the isotropic PDF.

Under the pseudospin approximation, where the atomic level *x*-*y* shear stress is allowed to take only one of the two quantized states, we established a connection between the stress correlation function $C(\vec{r})$ and a linear combination of SRPDFs $\Gamma(\vec{r})$. Strong resemblance between $C(\vec{r})$ and $\Gamma(\vec{r})$ is observed. We further proposed an idea to interpret the long-range stress correlation function as the manifestation of short-range Ising-like pseudospin interaction. One feasible form of interaction is presented and tested. In our view, this Ising pseudospin model could be a viable method to study stress correlation in liquids.

Although the current study focused only on the instantaneous spatial correlations, we can readily extend them to incorporate dynamical information. With extended parameters denoted as $C(\vec{r},t)$ and $\Gamma(\vec{r},t)$, we can examine the relaxation of their isotropic and anisotropic components. One of the key questions is whether or not these two components relax independently. This is because the isotropic and anisotropic modes may stem from different origins. Whereas the former is intimately connected to viscous phenomena of liquids, the latter could be due to Eshelby's inclusion effect [24, 32]. Because the Eshelby field does not have an isotropic component it does not directly contribute to viscosity. The contribution to viscosity arises indirectly through relaxation. These subjects will be addressed in future publications.

Acknowledgments

The authors thank J. S. Langer, J. R. Morris and J. Bellissard for useful discussions. This research has been supported by the U.S. Department of Energy, Office of Science, Basic Energy Sciences, Materials Science and Engineering Division.

Appendix: Spherical harmonics expansion on PDF

Let us start from the definition of PDF as expressed below

$$g(\vec{r}) = \frac{A}{N^2}\left\langle \sum_{i\neq j} \delta(\vec{r} - \vec{r}_{ij}) \right\rangle, \tag{A1}$$

where N is the number of particle and A is the area of the system. In 3D, the Dirac's delta function can be casted as

$$\delta(\vec{r} - \vec{r}_{ij}) = \frac{1}{r^2 \sin(\theta)} \delta(r - r_{ij})\delta(\theta - \theta_{ij})\delta(\varphi - \varphi_{ij}). \tag{A2}$$

Nonetheless the counterpart in 2D is different and is listed below

$$\delta(\vec{r} - \vec{r}_{ij}) = \frac{1}{r} \delta(r - r_{ij})\delta(\theta - \theta_{ij}). \tag{A3}$$

This result can be verified as following

$$\int \delta(\vec{r} - \vec{r}_{ij}) d\vec{r} = \int_0^{2\pi}\int_0^{\infty} r dr d\theta \delta(\vec{r} - \vec{r}_{ij}) = \int_0^{2\pi}\int_0^{\infty} r dr d\theta \frac{1}{r} \delta(r - r_{ij})\delta(\theta - \theta_{ij}) = 1. \tag{A4}$$

Next we perform spherical expansion on PDF following the standard procedure

$$g(\vec{r}) = \sum_{l,m} g_l^m(r) Y_l^m\left(\frac{\vec{r}}{|\vec{r}|}\right), \tag{A5}$$

where Y_l^m are the real spherical harmonics. To obtain explicit expression for $g_l^m(r)$, we multiple $Y_{l'}^{m'}$ on both sides of Eq. A5 and perform integration over Ω:

$$\int Y_{l'}^{m'}(\Omega) g(r,\Omega) d\Omega = \sum_{l,m} g_l^m(r) \int Y_{l'}^{m'}(\Omega) Y_l^m(\Omega) d\Omega. \tag{A6}$$

The spherical harmonics are mutually orthogonal meaning $\int Y_{l'}^{m'}(\Omega)Y_l^m(\Omega)d\Omega = 4\pi\delta_{ll'}\delta_{mm'}$ in 3D. However, for convenience, we prefer $\int Y_{l'}^{m'}(\Omega)Y_l^m(\Omega)d\Omega = 2\pi\delta_{ll'}\delta_{mm'}$ in 2D. Consequently the left hand side of Eq. A6 can be simplified as $2\pi g_{l'}^{m'}(r)$. As a result, we arrive at the following relationship,

$$g_l^m(r) = \frac{1}{2\pi}\int Y_l^m(\Omega)g(r,\Omega)d\Omega\,. \tag{A7}$$

Replacing Eq. A1 into Eq. A7 leads to

$$g_l^m(r) = \frac{1}{2\pi}\frac{A}{N^2}\left\langle \sum_{i\neq j}\int Y_l^m(\Omega)\delta(\vec{r}-\vec{r}_{ij})d\Omega \right\rangle. \tag{A8}$$

Next we substitute Eq. A3 into Eq. A8, then we get

$$g_l^m(r) = \frac{1}{2\pi r}\frac{A}{N^2}\left\langle \sum_{i\neq j}\int Y_l^m(\theta)\delta(r-r_{ij})\delta(\theta-\theta_{ij})d\theta \right\rangle, \tag{A9}$$

and further

$$g_l^m(r) = \frac{1}{2\pi r}\frac{A}{N^2}\left\langle \sum_{i\neq j} Y_l^m(\theta_{ij})\delta(r-r_{ij}) \right\rangle. \tag{A10}$$

Based on the general expression in Eq. A10, we can write explicitly that

$$g_0^0(r) = \frac{1}{2\pi r}\frac{A}{N^2}\left\langle \sum_{i\neq j}\delta(r-r_{ij}) \right\rangle, \text{ where } Y_0^0 = 1. \tag{A11}$$

$$g_2^{-2}(r) = \frac{\sqrt{2}}{\pi r}\frac{A}{N^2}\left\langle \sum_{i\neq j}\frac{x_{ij}y_{ij}}{r_{ij}^2}\delta(r-r_{ij}) \right\rangle, \text{ where } Y_2^{-2} = \sqrt{8}\frac{xy}{r^2} = \sqrt{2}\sin(2\theta). \tag{A12}$$

$$g_2^2(r) = \frac{\sqrt{2}}{2\pi r}\frac{A}{N^2}\left\langle \sum_{i\neq j}\frac{x_{ij}^2 - y_{ij}^2}{r_{ij}^2}\delta(r - r_{ij})\right\rangle, \text{ where } Y_2^2 = \sqrt{2}\,\frac{x^2 - y^2}{r^2} = \sqrt{2}\cos(2\theta). \qquad \text{(A13)}$$

$$g_4^{-4}(r) = \frac{2\sqrt{2}}{\pi r}\frac{A}{N^2}\left\langle \sum_{i\neq j}\frac{x_{ij}y_{ij}(x_{ij}^2 - y_{ij}^2)}{r_{ij}^4}\delta(r - r_{ij})\right\rangle, \text{ where } Y_4^{-4} = 4\sqrt{2}\,\frac{xy(x^2 - y^2)}{r^4} = \sqrt{2}\sin(4\theta). \text{ (A14)}$$

$$g_4^4(r) = \frac{\sqrt{2}}{2\pi r}\frac{A}{N^2}\left\langle \sum_{i\neq j}\frac{x_{ij}^2(x_{ij}^2 - 3y_{ij}^2) - y_{ij}^2(3x_{ij}^2 - y_{ij}^2)}{r_{ij}^4}\delta(r - r_{ij})\right\rangle \quad , \quad \text{where}$$

$$Y_4^4 = \sqrt{2}\,\frac{x^2(x^2 - 3y^2) - y^2(3x^2 - y^2)}{r^4} = \sqrt{2}\cos(4\theta). \qquad \text{(A15)}$$

References:

1. J.-P. Hansen and I. R. McDonald, *Theory of Simple Liquids* (Academic Press, Amsterdam, 2006) 3rd ed.
2. P. A. Egelstaff, *An Introduction to the Liquid State* (Oxford University Press, Oxford, 1994) 2nd ed.
3. J. L. Yarnell, M. J. Katz, R. G. Wenzel, and S. H. Koenig, Phys. Rev. A **7**, 2130 (1973).
4. B. A. Dasannacharya and K. R. Rao, Phys. Rev. **137**, A417 (1965).
5. A. Rahman, Phys. Rev. **136**, A405 (1964).
6. R. Evans and T. J. Slukin, J. Phys. C: Solid State Phys. **14**, 2569 (1981).
7. M. A. González and J. L. F. Abascal, J. Chem. Phys. **132**, 096101 (2010).
8. M. Mondello and G. S. Grest, J. Chem. Phys. **106**, 9327 (1997).
9. W. G. Hoover, D. J. Evans, R. B. Hickman, A. J. C. Ladd, W. T. Ashurst, and B. Moran, Phys. Rev. A **22**, 1690 (1980).
10. J. J. Erpenbeck, Phys. Rev. A **38**, 6255 (1988).
11. S. Hess and D. J. Evans, Phys. Rev. E **64**, 011207 (2001).
12. S. T. Cui, P. T. Cummings, and H. D. Cochran, Mol. Phys. **88**, 1657 (1996).
13. T. Egami, K. Maeda and V. Vitek, Phil. Mag. A **41**, 883 (1980).
14. V. A. Levashov, J. R. Morris and T. Egami, Phys. Rev. Lett. **106,** 115703 (2011).
15. V. A. Levashov, J. R. Morris, and T. Egami, J. Chem. Phys. **138**, 044507 (2013).
16. A. Furukawa and H. Tanaka, Phys. Rev. Lett. **103**, 135703 (2009).
17. A. Furukawa and H. Tanaka, Phys. Rev. E **84**, 061503 (2011).
18. J. Chattoraj and A. Lemaître, Phys. Rev. Lett. **111**, 066001 (2013).
19. A. Lemaître, Phys. Rev. Lett. **113**, 245702 (2014).
20. M. Tsamados, A. Tanguy, C. Goldenberg, and J. –L. Barrat, Phys. Rev. E **80**, 026112 (2009).
21. F. Leonforte, A. Tanguy, J. P. Wittmer, and J. –L. Barrat, Phys. Rev. B **70**, 014203 (2004).
22. I. Goldhirsch and C. Goldenberg, Eur. Phys. J. E **9**, 245 (2002).
23. C. Goldenberg, A. P. F. Atman, P. Claudin, G. Combe, and I. Goldhirsch, Phys. Rev. Lett. **96**, 168001 (2006).
24. B. Wu, T. Iwashita and T. Egami, Phys. Rev. E **91**, 032301 (2015).
25. M. P. Allen and D. J. Tildesley, *Computer Simulation of Liquids* (Oxford University Press, New York, 1987).
26. S. Plimpton, J. Comp. Phys. **117**, 1 (1995).
27. T. Egami and D. Srolovitz, J. Phys. F: Metal Phys. **12**, 2141 (1982).
28. T. Egami, S. J. Poon, Z. Zhang and V. Keppens, Phys. Rev. B **76,** 024203 (2007).
29. T. Egami, Progr. Mater. Sci. **56,** 637 (2011).
30. T. Egami and S. Aur, J. Non-Cryst. Solids **89**, 60 (1987).
31. V. A. Levashov, T. Egami, R. S. Aga, and J. R. Morris, Phys. Rev. B **78**, 064205 (2008).
32. J. D. Eshelby, Proc. Roy. Soc. London, Ser. A **241**, 376 (1957).
33. J. S. Langer, Phys. Rev. E **88,** 012122 (2013).

Figure captions:

Figure 1. (Color online) The SRPDF $g_{xy^+,0}(r,\theta)$ calculated from a liquid at $T^* = 1$. Panel (a) shows the contour plot while panel (b) illustrates the intensities along three representative directions, namely polar angle $\theta = 0^o$ (black dot dash), 45^o (blue dash), and 135^o (red).

Figure 2. (Color online) The isotropic (l = 0 mode) component of $g_{+,0}(\vec{r})$ in panel (a) and the anisotropic (l = 2, m = - 2 mode) component in panel (b) acquired from spherical harmonics expansion. The isotropic component is compared against total PDF and the anisotropic counterpart is compared with the derivate of total PDF after rescaling and phase shifting.

Figure 3. (Color online) Two-dimensional contour plots of $g_{+,+}(\vec{r})$ in panel (a) and $g_{+,-}(\vec{r})$ in panel (b) computed from liquid phase at $T^* = 1$.

Figure 4. (Color online) The comparison between isotropic components (l = 0 mode) of $g_{+,+}(\vec{r})$ and $g_{+,-}(\vec{r})$ in panel (a), sin(2θ) components (l = 2, m = -2 mode) in panel (b), and cos(4θ) components (l = 4, m = 4 mode) in panel (c). Note $g^{4,4}_{+,-}(r) = -g^{4,4}_{+,+}(r)$.

Figure 5. (Color online) The contour plots of $C(\vec{r})$ in panel (a), and $\Gamma(\vec{r})$ in panel (b) computed from liquid phase at $T^* = 1$. See text for their definitions.

Figure 6. (Color online) The comparisons between l = 0 modes of $\Gamma(\vec{r})$ and $C(\vec{r})$ in panel (a) and their l = 4, m = 4 modes in panel (b). A same factor is employed to rescale the results from $C(\vec{r})$ for both cases.

Figure 7. (Color online) The comparisons between l = 0 modes of $S_{+,+}(\vec{r})$ and $g_{+,+}(\vec{r})$ in panel (a), their sin(2θ) modes in panel (b), and cos(4θ) modes in panel (c). The same comparisons between $S_{+,-}(\vec{r})$ and $g_{+,-}(\vec{r})$ are shown in panels (e)-(f).

Figure 8. (Color online) The screening length determined from $|S_4(r)|$ as a function of temperature along with a power law fitting curve which extrapolates to diverge at T_0 = 0.74.

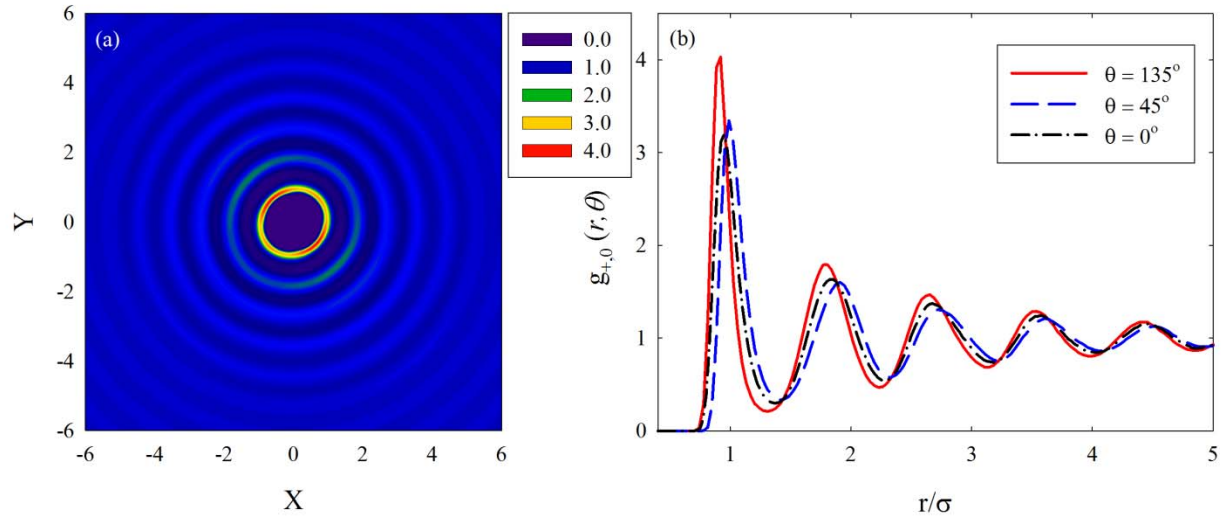
(a)
0.0
1.0
2.0
3.0
4.0
Y
X
(b)
θ = 135°
θ = 45°
θ = 0°
$g_{+,0}(r,\theta)$
r/σ

Fig. 1

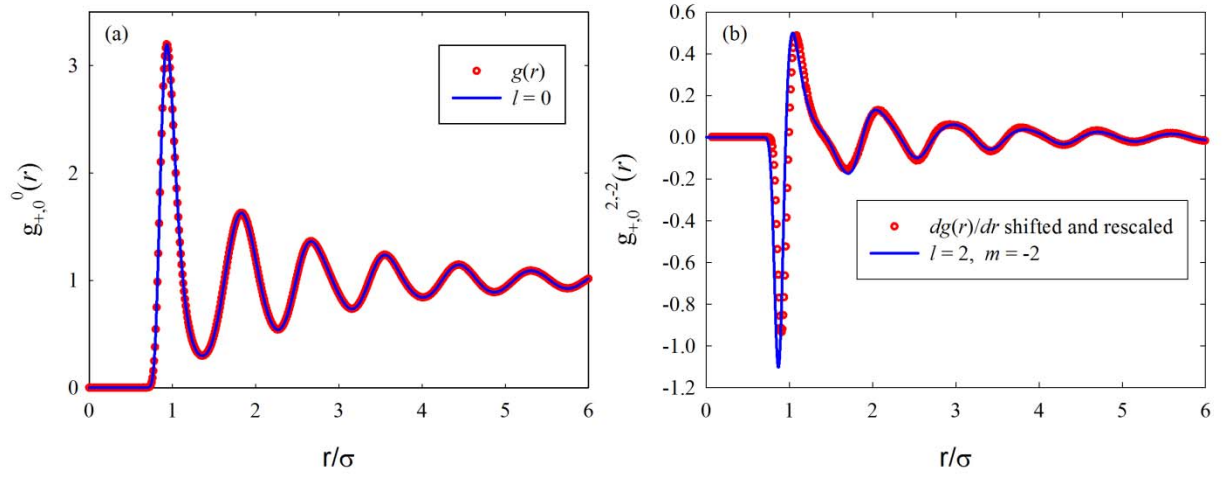
(a)
g(r)
l = 0
$g_{+,0}^{0}(r)$
r/σ
(b)
dg(r)/dr shifted and rescaled
l = 2, m = -2
$g_{+,0}^{2,-2}(r)$
r/σ

Fig. 2

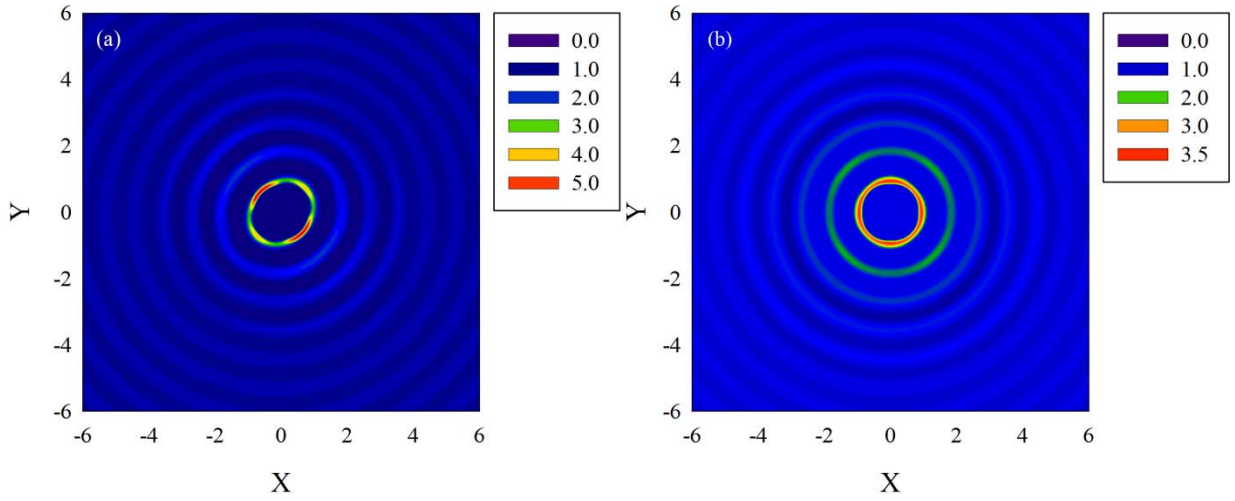

Fig. 3

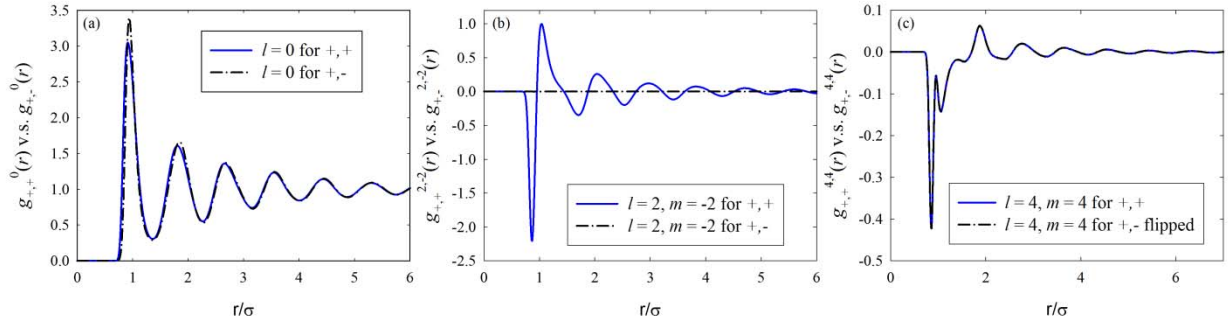

Fig. 4

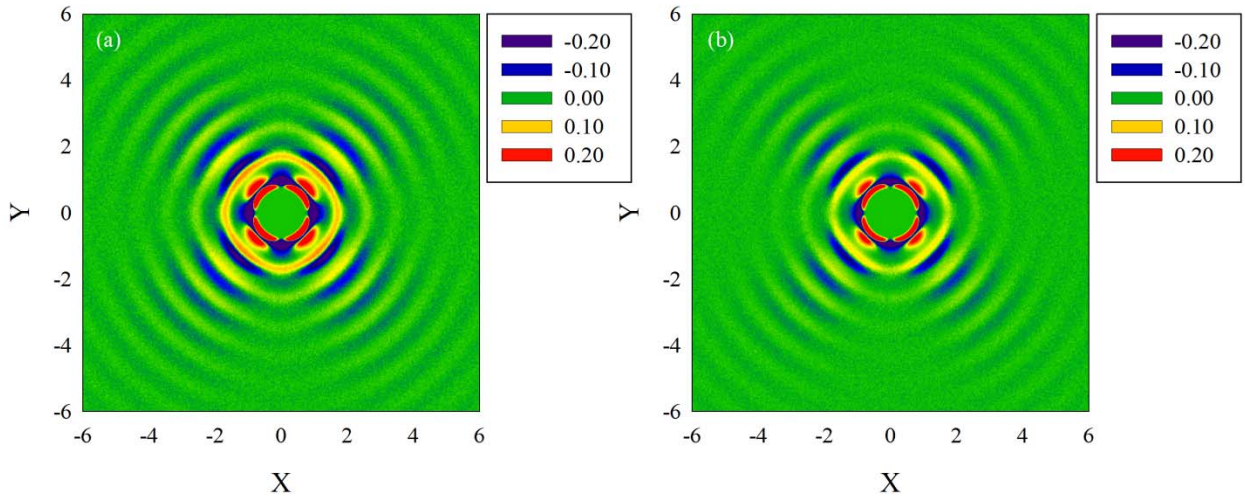

Fig. 5

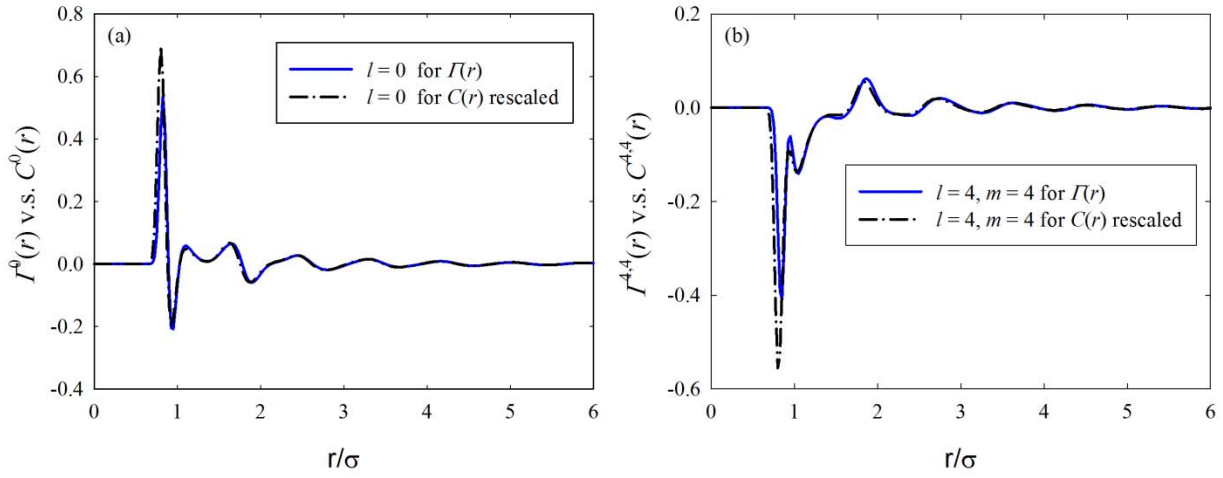
(a)
$l = 0$ for $\Gamma(r)$
$l = 0$ for $C(r)$ rescaled
$\Gamma^0(r)$ v.s. $C^0(r)$
r/σ
(b)
$l = 4$, $m = 4$ for $\Gamma(r)$
$l = 4$, $m = 4$ for $C(r)$ rescaled
$\Gamma^{4,4}(r)$ v.s. $C^{4,4}(r)$
r/σ

Fig. 6

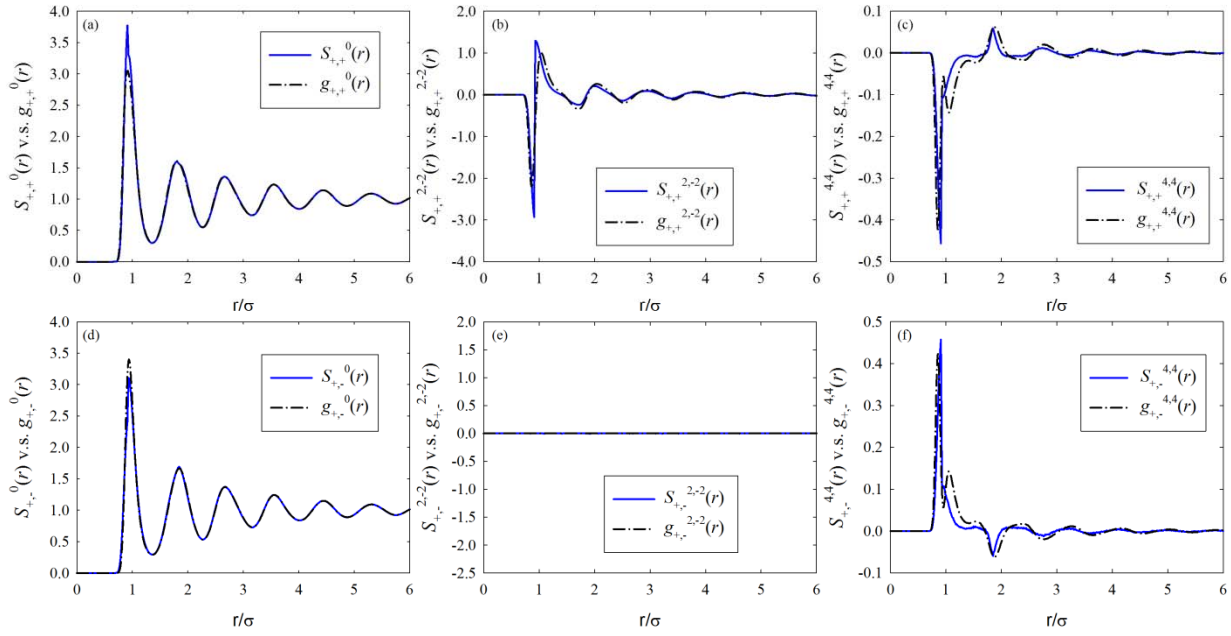
(a)
$S_{++}{}^{0}(r)$
$g_{++}{}^{0}(r)$
$S_{++}{}^{0}(r)$ v.s. $g_{++}{}^{0}(r)$
(b)
$S_{++}{}^{2,-2}(r)$
$g_{++}{}^{2,-2}(r)$
$S_{++}{}^{2,-2}(r)$ v.s. $g_{++}{}^{2,-2}(r)$
(c)
$S_{++}{}^{4,4}(r)$
$g_{++}{}^{4,4}(r)$
$S_{++}{}^{4,4}(r)$ v.s. $g_{++}{}^{4,4}(r)$
(d)
$S_{+-}{}^{0}(r)$
$g_{+-}{}^{0}(r)$
$S_{+-}{}^{0}(r)$ v.s. $g_{+-}{}^{0}(r)$
(e)
$S_{+-}{}^{2,-2}(r)$
$g_{+-}{}^{2,-2}(r)$
$S_{+-}{}^{2,-2}(r)$ v.s. $g_{+-}{}^{2,-2}(r)$
(f)
$S_{+-}{}^{4,4}(r)$
$g_{+-}{}^{4,4}(r)$
$S_{+-}{}^{4,4}(r)$ v.s. $g_{+-}{}^{4,4}(r)$
r/σ

Fig. 7

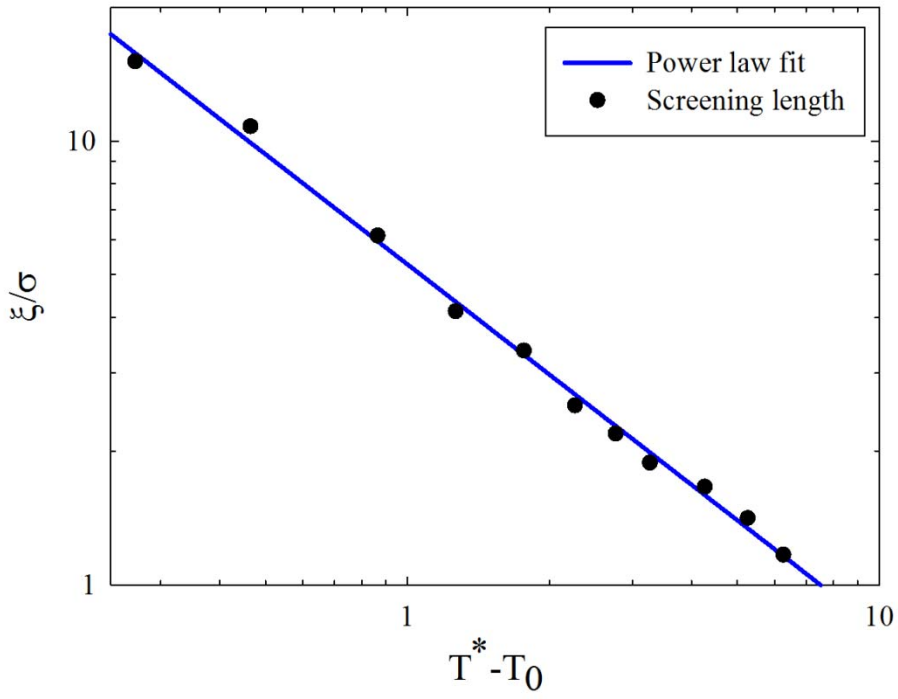

Fig. 8